New BIOTECHNOLOGY 78 (2023) 76–83

Contents lists available at ScienceDirect

New BIOTECHNOLOGY

journal homepage: www.elsevier.com/locate/nbt

# Site-specific antibody masking enables conditional activation with different stimuli

Roberta Lucchi, Maria C. Lucana, Montserrat Escobar-Rosales, Cristina Díaz-Perlas, Benjamí Oller-Salvia *

*Department of Bioengineering, Institut Químic de Sarrià (IQS), Universitat Ramon Llull, Via Augusta 390, 08017 Barcelona, Spain*

ARTICLE INFO

*Keywords:*
Conditionally-active antibody
Activatable antibody
Masked antibody
Polymer-protein conjugate
Light-sensitivity
Protease-sensitivity

ABSTRACT

Antibody therapeutics show great potential to treat a variety of diseases. Often, the dose that can be safely administered is limited by side effects that arise from the interaction with the target outside the diseased tissue. Conditionally-active antibodies provide an additional layer of selectivity to improve safety. Distinct external stimuli or internal cues enable different control strategies and applications. However, current antibody masking strategies have low transferability across stimuli. Here we propose a versatile approach to conditionally mask antibody derivatives and its application to a single chain variable fragment (scFv) against a receptor expressed on cancer stem cells in several tumours. Our strategy relies on the site-specific conjugation of a polymer to an engineered cysteine residue through a chemically-synthesised linker that can be cleaved in response to the target stimulus. We show that the masking efficiency depends on the conjugation site and the size of the mask. An optimised mask decreases antigen binding by up to 20-fold and affinity can be fully recovered upon activation by exposure to light at 365 nm or by incubation with matrix metalloproteinases overexpressed in solid tumours. This approach opens up the possibility to rapidly engineer antibodies activatable with any internal or external stimulus.

## Introduction

Monoclonal antibodies have shown high efficacy as therapeutics against several indications, such as oncology, immune disorders and infectious diseases, among others. Over 160 antibody-based therapeutics have been approved for clinical use by at least one regulatory agency and they are one of the most rapidly growing classes of drugs [1]. The high selectivity of antibodies for a target tissue relies on high expression levels of their antigen at the diseased site compared to other tissues. However, the number of targets with sufficient overexpression is very limited, and the vast majority of the approved antibody therapies are directed against less than 30 targets. Moreover, even antibodies that target antigens which are highly expressed at the diseased site have dose-limiting effects due to the engagement of the antigen in healthy tissues. One way to expand the pool of antigens that can be safely targeted is to add an additional layer of selectivity by rendering antibody binding conditional to particular stimuli. Reversibly-masked antibodies, which recover their ability to engage their target only after selective activation in the diseased tissue, can lead to an increased therapeutic window and may even enable new therapeutic modalities [2].

The field of conditionally-active or activatable antibodies has emerged within the last decade [3]. Therapeutic antibodies can be activated in response to a wide variety of stimuli, both internal, such as the presence of specific enzymes or pH, and external, such as light and small molecules. Three pH-sensitive antibodies are in clinical use [4–6] and several protease-sensitive antibodies are currently in clinical trials. However, all the approaches published in the literature show limited versatility. Some can only be applied to specific antibody formats or specificities and very few can be adapted to respond to different stimuli.

*Abbreviations:* AF647, Alexa Fluor® 647; APMA, 4-Aminophenylmercuric acetate; BSA, bovine serum albumin; CDR, complementary determining region; DCM, dichloromethane; DIC, N,N-Diisopropylcarbodiimide; DMF, N,N-dimethylformamide; DMSO, dimethyl sulfoxide; Fmoc, fluorenylmethoxycarbonyl; FPLC, fast protein liquid chromatography; IMAC, immobilised metal chelate ion affinity chromatography; mal, maleimide; LC-MS, liquid chromatography-mass spectrometry; MMP, matrix metalloproteinase; QTOF, quadrupole time of flight; scFv, single-chain variable fragment; SEC, size exclusion chromatography; TCEP, Tris(2-carboxyethyl)phosphine; UHPLC, Ultra-high-performance liquid chromatography; WB, Western Blot; WT, wild type.

* Corresponding author.
*E-mail address:* benjami.oller@iqs.url.edu (B. Oller-Salvia).

https://doi.org/10.1016/j.nbt.2023.10.004
Received 21 July 2023; Received in revised form 17 September 2023; Accepted 7 October 2023
Available online 10 October 2023

Most antibody masking strategies reported to date rely on the extension of the protein N-terminus with a blocking moiety. For instance, XTENylated® antibodies consist in fusing a single chain antibody variable fragment (scFv) with a long unstructured sequence [7]. This extension enables a substantial reduction in antibody binding. Antibody derivatives masked with this approach have shown promising results and have recently entered clinical trials (ClinicalTrials.gov Identifier: NCT05356741). Since fusion proteins restrict the position of the mask to the N-terminus, even if small masks have been reported for particular antibodies [8], large polypeptides (250-500 amino acid residues) are generally required [7]. Furthermore, applicability of recombinant polypeptide masks is limited to using proteases as an activation cue.

In this work, a new strategy to engineer activatable antibodies that can be adapted to different activation stimuli has been developed. The proposed approach relies on the site-specific conjugation of a flexible and hydrophilic polymer near the complementary determining regions (CDRs) to reversibly mask the antibody by steric hindrance (Fig. 1). First, the production of an scFv with a suitable reactive cysteine was set up. Then, the extent to which masking efficiency can be modulated through the conjugation site and the polymer size was investigated. Finally, responsiveness to two different activation stimuli, namely light and proteases, was implemented to unmask the scFv and recover binding affinity.

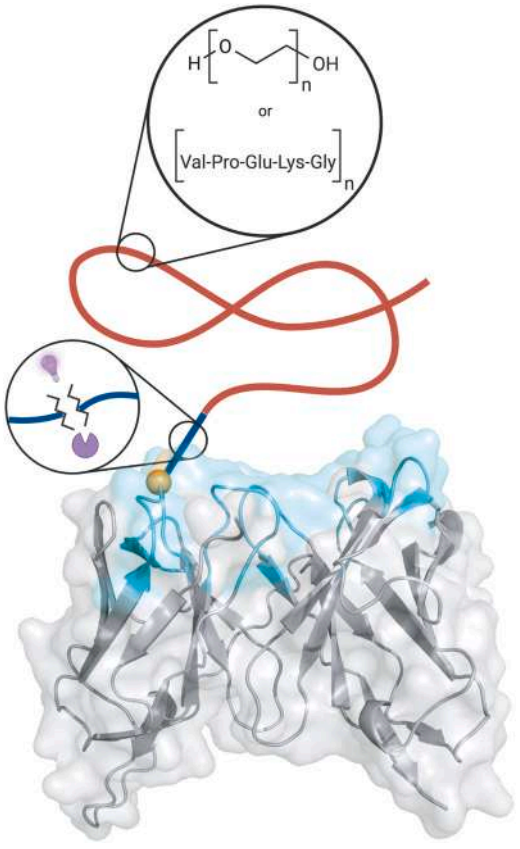


**Fig. 1.** Schematic representation of the new approach to generate conditionally active scFvs presented here. A polymer is site-specifically conjugated to a Cys residue (orange sphere), engineered at a selected position in the complementary determining regions (CDRs, in aquamarine). The mask is tethered to the scFv via a linker synthetised to be cleaved in response to a defined stimulus, such as light or proteases.

## Materials and methods

### *General materials and reagents*

LB broth was purchased from NZYTech (Lisbon, Portugal), sodium chloride from Scharlab (Barcelona, Spain), potassium chloride from Panreac Química (Barcelona, Spain), Tris(2-carboxyethyl)phosphine (TCEP) from EMD Millipore (Darmstadt, Germany), while Trizma base, potassium phosphate monobasic, sodium phosphate dibasic, kanamycin sulphate, ethylenediaminetetraacetic acid (EDTA), 2-mercaptoethanol, urea, phenylmethanesulfonyl fluoride (PMSF), L-glutathione reduced and L-glutathione oxidised were purchased from Sigma Aldrich (Milwaukee, WI, USA). Reagents for solid-phase peptide synthesis include: RinkAmide ChemMatrix® resin purchased from PCAS BioMatrix Inc. (St-Jean-sur-Richelieu, Quebec, Canada), 2-chlorotrytil chloride resin, Fmoc-protected amino acids, 4-{4-[1-(9-Fluorenylmethyloxycarbonylamino)ethyl]-2-methoxy-5-nitrophenoxy} butanoic acid, and OxymaPure® from Iris Biotech (Marktredwitz, Germany), N,N-Diisopropylcarbodiimide (DIC) from Sigma Aldrich (Milwaukee, WI, USA), trifluoroacetic acid (TFA) from Apollo Scientific (Cheshire, UK), dichloromethane (DCM) from VWR Chemicals (Radnor, PA, USA), and N,N-dimethylformamide (DMF) and pyperidine from Carlo Erba Reagents (Emmendingen, Germany).

### *scFv construct and Cys-scanning library preparation*

The anti-CD133 gene was kindly provided by Dr. Jayanth Panyam in a pET28c vector with kanamycin resistance [9]. The c-terminal FLAG- and $His_{12}$-tags were introduced by PCR in two amplification reactions using long reverse primers (Suppl. Table S1). To increase amplification yield, 5% DMSO was added to the PCR reaction. The amplified product was digested with *Nco*I-HF and *Not*I-HF restriction enzymes (New England Biolabs, Ipswich, MA, USA), as was the pET28c vector, and ligation was performed with T4 DNA ligase (New England Biolabs, Ipswich, MA, USA), following manufacturer's instructions. For the mutant library, Cys residues were site-specifically mutated into selected positions along the scFv sequence by Quick-change mutagenesis using partially-overlapping primers (Suppl. Table S2). Template DNA was digested with *Dpn*I before transforming into chemically competent DH5a cells. All cloning procedures were confirmed by Sanger sequencing.

### *scFvs expression and purification from inclusion bodies*

BL21(DE3) *E. coli* chemically competent cells were transformed with the cloned plasmids and grown in LB + 50 mg/mL kanamycin at 37 °C with shaking overnight. On the following day, pre-inoculum was diluted to 0.1 $OD_{600}$ and allowed to grow at 37 °C and shaking until $OD_{600}$ reached at least 0.8. At this point, 750 µM Isopropyl β-d-1-thiogalactopyranoside (IPTG, Neo Biotech, Nanterre, France) were added to the culture and scFvs expression was carried out at 30 °C and 150 rpm overnight. Cells were harvested by centrifugation at 6000 *g* for 15 min at 4 °C. Pellets were resuspended in lysis buffer (50 mM TRIS-HCl pH 8.0, 1 mM EDTA, 150 mM NaCl, 1% Triton X-100 and 1 mM PMSF) and intracellular content was released by sonication at 40% amplitude, with 25 s ON and 30 s OFF pulses, for a total of 10 min on ice. Lysis suspension was clarified centrifuging at 25,000 *g* for 25 min at 4 °C. Inclusion bodies were solubilised by gentle agitation at 4 °C in denaturation buffer (50 mM TRIS-HCl pH8.0, 50 mM NaCl, 7 M urea and 5 mM 2-mercaptoethanol) for 45 min to 1 h, followed by centrifugation at 25,000 *g*, for 25 min at 4 °C. From the supernatant, denatured scFv was purified by Immobilised Metal Chelate Affinity Chromatography (1 mL IMAC HisTrap™ HP column, Cytiva, Amersham, UK) on a fast protein liquid chromatography system (FPLC, BIO-RAD NGC, BIO-RAD, Hercules, CA, USA). Purified scFvs were refolded by dialysis adapting the protocol in [10]. Briefly, the protein was dialysed against

buffers with decreasing urea concentration, starting from 45 mM TRIS-HCl pH8.0, 1 mM EDTA, 1 mM GSH, 0.2 mM GSSG and 6 M urea, then reducing urea to 4, 2, 1, 0.5 and 0.2 M. Urea was removed completely by dialysing against 45 mM TRIS-HCl, 1 mM EDTA and 150 mM NaCl. Eventual precipitate was removed by centrifugation at 18,000*g* for 10 min at 4 °C. The refolded protein was analysed by SDS-PAGE and LC-MS. Samples were analysed using the Q-TOF X500B connected to an Exion LCAD chromatograph. The analysis was performed using the BioResolve RP mAb (150 ×2.1 mm×2.7 μm, Waters, Milford, MA, USA) column and applying a 5–95% gradient acetonitrile (0.1% formic acid) in water (0.1% formic acid) in 5 min. Q-TOF MS was operated in the positive ion mode for the analysis. The mass spectra were recorded across the range of 100–3000 Da with a fixed collision energy of 5 V. Data acquisition and evaluation was performed using SCIEX OS software.

*Stimuli-sensitive linkers synthesis*

All the linkers were synthetised via manual solid-phase peptide synthesis (SPPS). The synthesis was performed in polypropylene syringes with a polypropylene porous filter, mounted on top of a vacuum manifold for quick solvent elimination. A Rink amide AM resin (0.65 mmol/g) for the protease-sensitive linker and a Chlorotrytil resin (1.4 mmol/g) for the photo-sensitive linker were used. Fmoc-protected amino acids and reagents were subsequently coupled following standard protocols. Briefly, after washing the resin, N-terminal Fmoc was deprotected with 20% piperidine solution in DMF. Then, 4 eq of the following Fmoc-protected residue were activated with 4 eq DIC and 4 eq of OximaPure® to avoid racemization. Coupling reaction was allowed to proceed at RT for 1 h in DMF. Following each step, excess reagents and by-products were removed washing multiple times with DCM and DMF. Ninhydrin test was used to confirm correct coupling and Fmoc-deprotection, whereas chloranil test was used to detect secondary amines.

*Cleavage from the resin and side chain deprotection of the linkers*

After deprotecting the Fmoc from the last residue, the resin was washed several times with DCM and DMF and then allowed to dry for 15 min. The dried resin was collected in a falcon tube and incubated for 3 h at RT in the cleavage cocktail, made of TFA, DCM, ethanedithiol, water and triisopropylsilane in the following proportions 94:0:2.5:2.5:1 (v/v) for the protease-sensitive linker and 40:54:2.5:2.5:1 (v/v) for the photo-sensitive linker. The solvent was then evaporated under inert atmosphere. The peptide was precipitated by adding diethyl ether at 0 °C and centrifuging at 5000 *g* for 5 min at 4 °C. The process was repeated three times to remove any non-peptidic impurity. The cleaved peptides were solubilised in 50% acetonitrile in water with 0.1% TFA, separated from the resin by filtration through 0.45 μm filters and lyophilised.

*Stimuli-sensitive linkers purification and characterisation*

The lyophilised peptides were resuspended in water and purified using an Aeris Peptide XB-C18 100 LC Column (250 ×21.2 mm, 5 μm, Phenomenex, Torrance, CA, USA) mounted on an Agilent 1260 Infinity II system with ChromScope software, a 1260 VWD, a 1260 Preparative Binary Pump, a 1260 Column Organizer and a 1290 Preparative Fraction Collector. Purification was carried out in 5–95 gradient of acetonitrile (0.1% TFA) in water (0.1% TFA), with a flow of 20 mL/min. The peaks containing the peptide were identified using a MALDI-TOF Bruker Biotyper MBT smart, pooled together and lyophilised. Peptides purity was confirmed via UHPLC analysis.

*Stimuli-sensitive linkers cleavage analysis*

The photo-sensitive linker at 1 mM concentration was irradiated under a UV lamp at 15 cm distance and light at 365 nm with a measured irradiance of 1.7 mW/cm$^2$. Samples were collected at 5, 15, 30, 45 min, 1, 2 and 4 h, and diluted to 100 μM for analysis in the UHPLC. For the protease-cleavable linker, the MMP2 and MMP9 zymogens (Enzo Life-Science) at 1.6 μM were previously activated in Tris-Triton-Calcium buffer in the presence of 250 nM 4-Aminophenylmercuric acetate (APMA, Sigma Aldrich) for 1 or 5 h at 37 °C, respectively. After activation, the enzymes were diluted to 200 nM in the presence of 1 mM of the protease-sensitive linker (1:5000 enzyme:peptide) and incubated at 37 °C. Samples were taken at 0.5, 1, 1.5 and 2 h and diluted to 50 μM for analysis in UHPLC.

*Stimuli-sensitive linkers conjugation to PEG*

30 kDa mPEG-mal (Laysan Bio, Arab, AL, USA) was resuspended at 0.1 mM in water and reacted with 5 eq of photo- or protease-sensitive linker, in the presence of a 8 eq of triethylamine. Reaction was incubated for 2 h at RT, after which free Cys residues were capped with 20 eq of 2-mercaptoethanol (Sigma Aldrich, Milwaukee, WI, USA). Excess 2-mercaptoethanol was removed by gel filtration purification on a PD Miditrap column (GE Healthcare, Chicago, IL, USA), collecting fractions of 2–3 drops each. Fractions with highest concentration of PEG were pooled. 20 eq of 4-maleimidobutyric acid N-hydroxysuccinimide ester (mal-NHS, BLDpharm, Shanghai, China) were added to the reaction to functionalise the N-terminus of the peptide with maleimide and left to react for 2 h at RT. Finally, functionalised PEG was purified by gel filtration purification on a PD Miditrap column (GE Healthcare, Chicago, IL, USA) and lyophilised.

*Analytical UHPLC analysis*

Linkers purity and cleavage, as well as stimuli-responsive mask synthesis were analysed by reverse-phase UHPLC on a SunFire C18 column (100 Å, 3.5 μm, 4.6 mm × 150 mm, Waters) connected to an Agilent 1260 Infinity II system with ChromoScope software (1260 DAD W*R*, 1260 Vial Sampler and 1260 Flexible Pump). The flow was set to 0.6 mL/min using a standard 5–95% acetonitrile (0.1% TFA) in water (0.1% TFA) gradient over 12 min.

*Masks conjugation to scFv and purification*

scFvs were first reduced with at least 20 eq of TCEP for 2 h at RT. Reduced scFvs were buffer exchanged to PBS using a PD Miditrap column, while simultaneously removing the TCEP. Conjugation was carried out incubating with 25 eq of the mask, cleavable or uncleavable, for 2 h at RT. The scFv conjugated to the 5 kDa protease-cleavable zwitterionic peptide (Peptide Synthesis Core Facility, UPF) was used as such in the following experiments. The other samples were purified by size-exclusion chromatography (SEC) on an Enrich SEC 70 (BIO-RAD, Hercules, CA, USA) column, connected to a BIO-RAD NGC FPLC. After purification, when needed, samples were concentrated using 10 kDa MWCO 0.5 mL Amicon Ultra centrifugal filter devices (EMD Millipore, Darmstadt, Germany).

*Cell culture*

HeLa and Caco2 cells were cultured in DMEM High Glucose medium (BioWest, Nuaillé, France) supplemented with 10% foetal bovine serum (FBS, VWR Life Science Seradigm), 2 mM L-glutamine (BioWest, Nuaillé, France) and antibiotics (60 and 100 mg/L of penicillin and streptomycin respectively, Biowest, Nuaillé, France). Cells were cultured in T75 flasks until 80% confluence at 37 °C and 5% $CO_2$, then passaged. All work performed with human cells follow the ethical

principles and EU Directive 2004/23/EC.

*Cell binding experiments*

HeLa or Caco2 cells were seeded at $1 \times 10^4$ cells/well in 96-well plates. In the case of HeLa cells, one day after seeding, they were transfected with pCMV3-C-GFPSpark® Vector (SinoBiological, Beijing, China) using *Trans*IT-HeLaMONSTER® (Mirus Bio, Madison, WI, USA) and following manufacturer's instructions. Briefly, a transfection mix with 100 ng/well of plasmid, 0.2 µL/well of *Trans*IT reagent and 0.2 µL/well of HeLaMONSTER reagent in OPTI-MEM was prepared. 10 µL of this solution were added drop-wise to 100 µL of complete DMEM in each well. After overnight incubation, medium was changed to fresh complete DMEM. Cell binding assays were performed 48 h after transfection as follows: upon washing away the medium, cells were incubated with 50 µL of scFv at different dilutions in PBS + 1% bovine serum albumin (BSA, Sigma Aldrich, Milwaukee, WI, USA) for 1 h on ice; scFv solution was washed and replaced with 50 µL/well of a 1:1600 dilution of Alexa Fluor® 647 anti-DYKDDDDK Tag Antibody (BioLegend, San Diego, CA, USA) in PBS + 1% BSA, incubating for 45 min on ice. Following removal of the secondary antibody solution, cells were detached with 25 µL/well of Trypsin-EDTA (Gibco) for 5 min at 37 °C, after which trypsin was inactivated by adding 100 µL/well of complete DMEM with 33% (v/v) formalin. Cells were analysed with an Agilent NovoCyteflow cytometer, detecting at 488 nm the cells expressing the transfected construct and at 640 nm the cells with AF647-conjugated antibody on the surface. Data was analysed plotting the percentage of $AF647^+$-cells amongst the $GFP^+$ ones against the concentration of the scFv.

## Results and discussion

*Production and characterisation of the scFv*

The scFv format was selected because it is the minimal antibody format with both variable domains; thus, masking methods developed on scFvs may be readily transferred into other antibody formats. In particular, the selected scFv targets CD133, a biomarker for cancer stem cells in brain, prostate, colorectal and ovarian cancers, among others, but also expressed in several types of healthy cells [11].

An efficient expression system of the scFv in the cytoplasm of *E. coli* was set up. In order to facilitate detection and purification, the scFv was modified to include a FLAG-tag and a $His_{12}$-tag at the C-terminus (Suppl. Table S3). To maximise production yield, the scFv was expressed insolubly, purified from inclusion bodies, and refolded by dialysis, with a final yield of 8 mg/L of culture after refolding. The refolding process was carried out in the presence of both oxidised and reduced glutathione to favour formation of the correct cysteine pairs, keeping the pH constant at 8.0, while the concentration of denaturing agent was decreased step-wise. The purity of the protein was confirmed on SDS-PAGE (Suppl. Fig. S1) and the expected mass was identified by LC-MS analysis, confirming formation of two disulphide bridges (Fig. 2a).

In order to assess activity of the refolded scFv, the binding to HeLa cells transfected with a plasmid encoding for a CD133-GFP fusion protein was studied via flow cytometry. Fusion of GFP to the target receptor enabled gating for cells expressing high levels of CD133. From this experiment we calculated an apparent $K_D$ of 0.43 nM (Figs. 2b-c and S2).

*Effect of conjugation site and mask size on masking efficiency*

Antibody masking strategies based on steric hindrance mostly rely either on stochastic polymer conjugation or modification of the N-terminus. While the first approach yields heterogeneous mixtures and enables limited modulation capacity of binding affinity [12–14], the latter may require very large masks to significantly decrease affinity and enables only activation by proteases [7,15,16]. The N-terminus is relatively distant (2–3 nm) from the complementary determining region

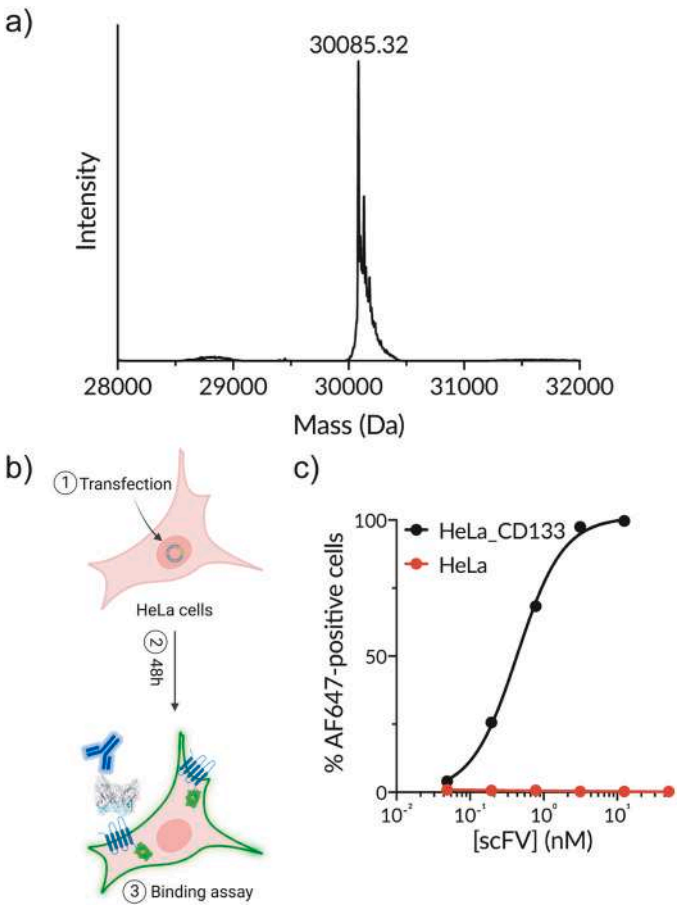


**Fig. 2.** Characterisation of the anti-CD133 scFv. a) Deconvoluted mass spectrum shows the expected mass accounting for the 4 Da loss after formation of the two disulphide bridges. b) Schematic representation of the experimental set-up for the binding assays. c) The refolded scFv shows specific binding with sub-nanomolar $K_d$ to HeLa cells upon transfection with the CD133 antigen.

(CDR) most commonly engaged in antigen binding, namely the CDR3 on the heavy chain (HCDR3). Therefore, we hypothesised that locating the mask closer or inbetween the CDRs might provide higher masking capacity. Hence, the extent to which the conjugation site influenced the masking efficiency needed to be assessed. To this end, several residues were mutated to cysteine to enable site-specific conjugation of the masking moiety through thiol-maleimide chemistry, although the strategy proposed could easily implement other site-specific conjugation methods [17]. Since no crystal structure was available for this scFv, a model of the structure was generated with AlphaFold2 [18] and used to guide the rational selection of conjugation sites, bearing in mind the limitations in the prediction of the loop conformations. The selected residues were located either in the more conserved loops flanking the CDRs or in the CDRs themselves, excluding the CDR3 from both chains (Figs. 3a and S3). The residues selected as anchor sites had side chains oriented towards the solvent to maximise reactivity with the mask.

All the Cys mutants were produced following the protocol we developed for the WT scFv. LC-MS analysis of the variants highlighted the presence of another peak corresponding to the scFv with the substituted Cys capped by the glutathione used during the refolding process. To ensure availability of the thiol group for conjugation, the refolded protein was first reduced with TCEP. LC-MS analysis of the reaction showed that incubation with at least 10 eq of TCEP for 2 h at 25 °C was needed to achieve full reduction of the scFv (Suppl. Fig. S4). The reduced Cys was then free to react with the selected mask (Fig. 3b and Suppl. Fig. S5).

The first screenings were performed using 10 kDa

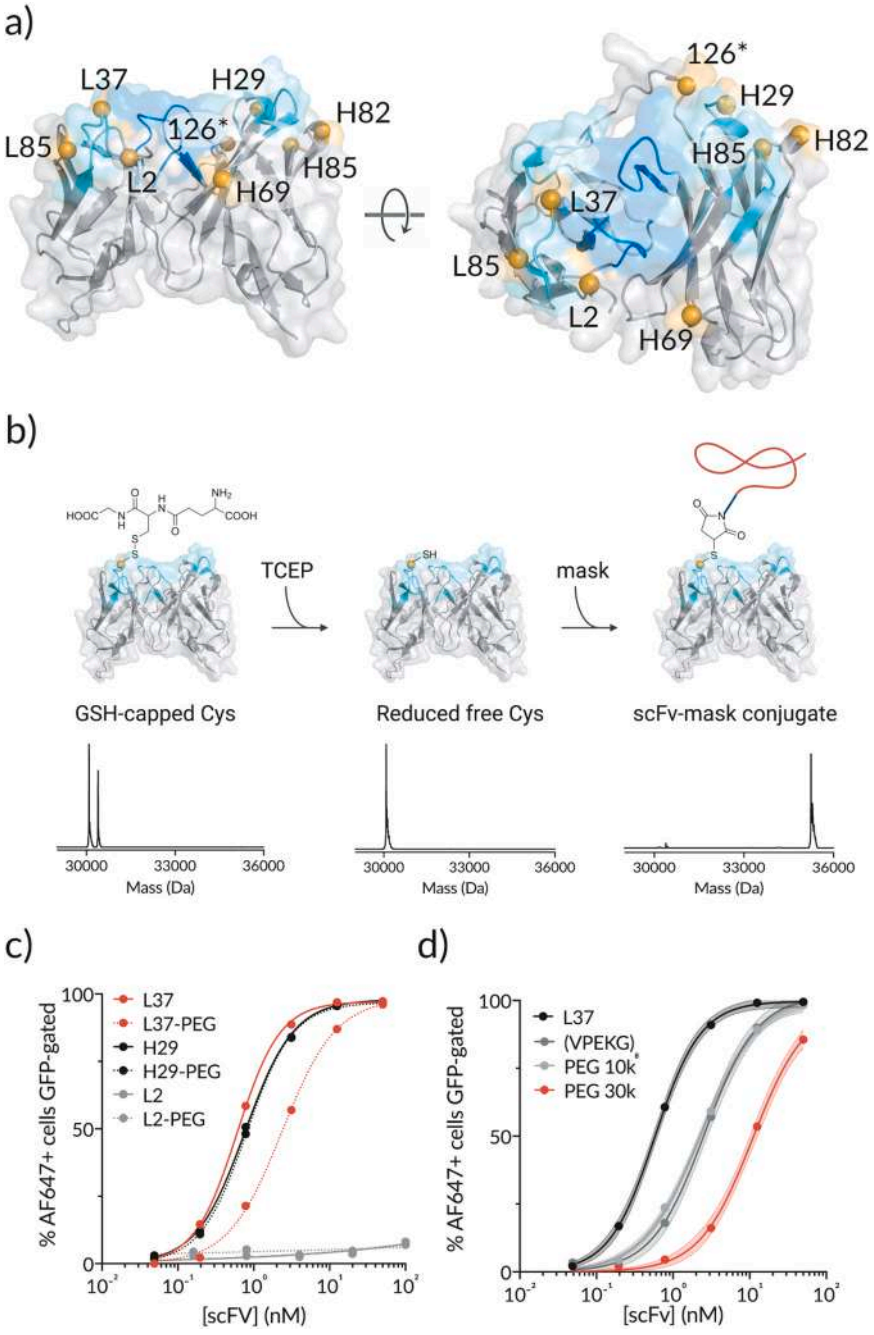


**Fig. 3.** Development of the masking strategy. a) Side and top view of the AlphaFold2 model of the anti-CD133 scFv. CDRs 1 and 2 are coloured in aquamarine and CDRs 3 in blue. The positions selected as conjugation sites for the masking moiety are represented as orange spheres and labelled according to their IMGT numbering, with L for light chain and H for heavy chain. The position marked as 126* is outside of the VL and VH domains and was numbered based on the position in the primary sequence. b) Schematic representation of the conjugation to the masking moieties. scFv was first reduced with TCEP to free the engineered Cys for the reaction with the maleimide-functionalised mask. Reduction and conjugation were confirmed by LC-MS analysis. c) Binding of different Cys mutants, conjugated or not to 10 kDa PEG. The results for three representative mutants are plotted in this graph. Data for all mutants is represented in Fig. S6c-e. d) Binding of L37 conjugated to masking moieties of different sizes, as measured by flow cytometry. Filled area indicates the 95% confidence interval for the fitted values. This set of data is representative of 2 independent experiments.

polyethyleneglycol (PEG) polymer as a mask (Suppl. Fig. S6a). After the conjugation, samples were purified by SEC to separate the masked scFv from the unconjugated protein (Suppl. Fig. S6b). Binding assays on CD133-transfected HeLa cells confirmed that conjugation site influenced masking efficiency (Fig. 3c or Suppl. S6c-e and Suppl. Table S5). For most of the mutants the introduction of the Cys alone did not significantly affect binding affinity. Two mutants had no measurable affinity; these mutations were close to the N-terminus (L2) and in the scFv framework (H69), probably impacting on translation or refolding (Suppl. Fig. S6c). For the mutations on the linker (126 *), on the HCDR1 (H29) or close to it spatially (H85, Fig. 3a), no significant difference in affinity was observed between masked and unmasked scFv (Suppl Fig. S6d). For the three mutants L37, L85 and H82, a substantial increase in the $K_D$ of the PEGylated scFv was observed compared to the unmasked mutant to different extents (Suppl. Fig. S6e). Although L85 and H82 are outside the CDRs, mutating these positions decreased antigen binding. Conversely, modification of L37, a serine on LCDR1 close to the anchor point with the β-sheet scaffold, had no effect on the $K_D$. Moreover,

conjugating the mask to L37 provided the largest shift in binding with respect to the unmasked scFv [19,20]. Although the selected position could be transferable to other antibodies, because LCDR1 is less frequently involved in binding than other CDRs, screening of several positions might be necessary to ensure maximal binding and masking efficiency. Since L37 provided the tightest binding and largest masking effect, we proceeded to investigate the masking efficiency of polymers of different sizes conjugated to this position.

Three masking moieties, with molecular weights of 5, 10 and 30 kDa, were conjugated to the scFv (Suppl. Fig. S7). It was observed that, although the smaller masks already provided a certain degree of inactivation, the masking capacity increased with size (Fig. 3d and Suppl. Table S5). Interestingly, the 5 kDa zwitterionic peptide and the 10 kDa PEG had a similar effect, around 6 and 4-fold inhibition respectively, despite the latter being twice the size of the first. The chosen peptide motif, $[VPEKG]_8$, is intrinsically unstructured [21], with paired anionic and cationic residues for stealth and proline residues to partly decrease the flexibility. The lower conformational flexibility of this zwitterionic peptide might explain why a masking efficiency similar to that of a PEG twice its size is achieved. Finally, the 30 kDa PEG resulted into a reduction in affinity of 20 folds. This confirmed that the size and nature of the masking moiety greatly affect the masking efficiency.

### *Development of a photo-activatable PEGylated scFv*

After confirming that site-specific conjugation of a polymer to the scFv paratope could be applied to mask the scFv binding its receptor, we proceeded to demonstrate that binding could be rescued upon unmasking. Light is an interesting activation stimulus because it enables high temporal and spatial resolution. Moreover, it could be useful to activate targeted therapies for dermatological malignancies [22,23], or even for deeper malignancies by using fibre optic-coupled LED systems [24]. In particular, UVA light at 365 nm has sufficient penetration for the treatment of dermal and subdermal diseases [25]. To make the mask responsive to light, a linker was designed, that bears a photocleavable nitrobenzyl moiety that can be cleaved efficiently upon irradiation at 365 nm (Fig. 4a). The linker was synthetised via solid phase peptide synthesis, with a Cys residue to conjugate it to a maleimide-bearing PEG and an N-terminal Gly to stabilise the photolinker. Time-dependent cleavage of the synthetised photolinker was followed by UHPLC and full cleavage was achieved after shining light at 365 nm for 2 h (Figs. 4b and S8a).

The photolinker was conjugated to the 30 kDa mPEG-mal in solution, followed by functionalisation of the N-terminal amine with maleimide. Each step of the synthesis of the photo-cleavable mask was followed by reverse-phase UHPLC and the product was purified by gel filtration (Suppl. Fig. S8b-c). After purification, the mask was conjugated to the L37 mutant, minimising light exposure, and its cleavage upon UV light irradiation was evaluated by SDS-PAGE and WB analysis (Fig. 4c and Suppl. Fig. S8d). The binding capability of the photo-sensitive masked-scFv before and after shining light was assessed by flow cytometry on CD133-transfected HeLa cells. Complete recovery of the binding affinity was observed after only one hour irradiation with light at 365 nm (Fig. 4d).

### *Development of a protease-activatable PEGylated scFv*

Until now, few antibody masking methods have shown transferability across different stimuli, and these have been mostly designed for diagnostic applications [3,26,27]. Aiming to show that our approach can be readily adapted to other stimuli, a linker sensitive to proteolysis was designed. Proteases are known to be overexpressed in many pathologies, including autoimmune, cardiovascular, neurogenerative diseases, as well as cancer. Many proteases have been exploited to ensure selective activation of prodrugs at the diseased site, to improve specificity and reduce side effects. Matrix metalloproteases (MMPs) are upregulated in the tumour microenvironment of several different cancer types. In particular, MMP2 and MMP9 have been found in breast [28], colorectal [29], brain [30] and lung [31] cancers among others. The altered activity of MMPs has already been explored as an activation cue for small molecule prodrugs [32,33], as well as in other approaches to make conditionally-active antibodies [34,35].

To implement protease sensitivity in the mask design, a peptide was synthetised with a sequence known to be cleaved by both MMP2 and MMP9: GPLGIAGQ [36]. To enable conjugation of the peptide to the PEG linker, a cysteine residue was added towards the C-terminus of the cleavable sequence (Fig. 5a). Similarly to the photo-sensitive linker, cleavage of the selected sequence was confirmed by reverse-phase

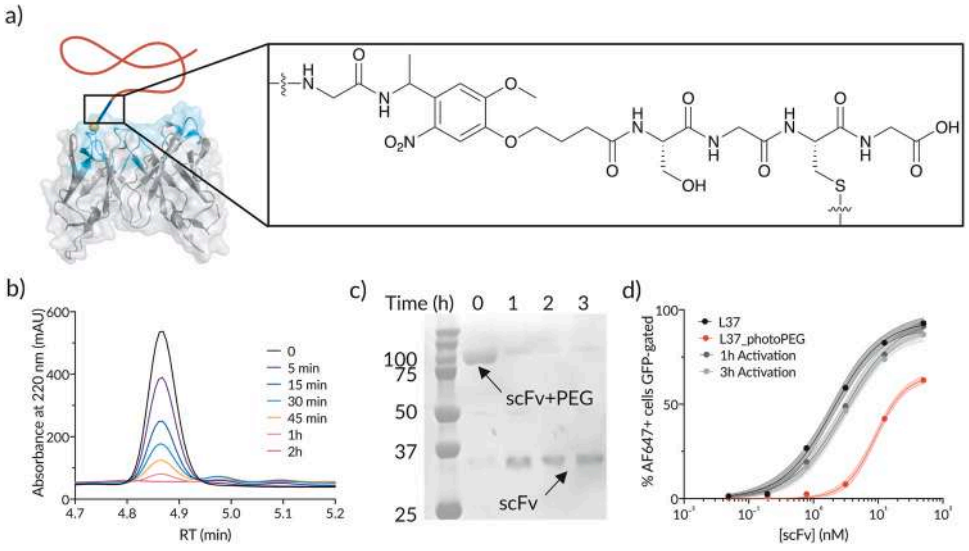


**Fig. 4.** Engineering light sensitivity into the masked scFv. a) Sequence of the photo-labile linker. b) Disappearance of the peak of the synthetised photo-labile linker over time upon irradiation at 365 nm, as analysed by reverse-phase UHPLC. Data for the whole cleavage analysis is represented in Fig. S8a. c) Coomassie-stained SDS-PAGE gel showing cleavage of photo-sensitive PEG conjugated to L37 after irradiating with light at 365 nm. d) Binding of the scFv conjugated to photo-cleavable PEG with and without exposure to light at 365 nm, as assessed by flow cytometry. Filled area indicates the 95% confidence interval for the fitted values. This set of data is representative of 3 independent experiments.

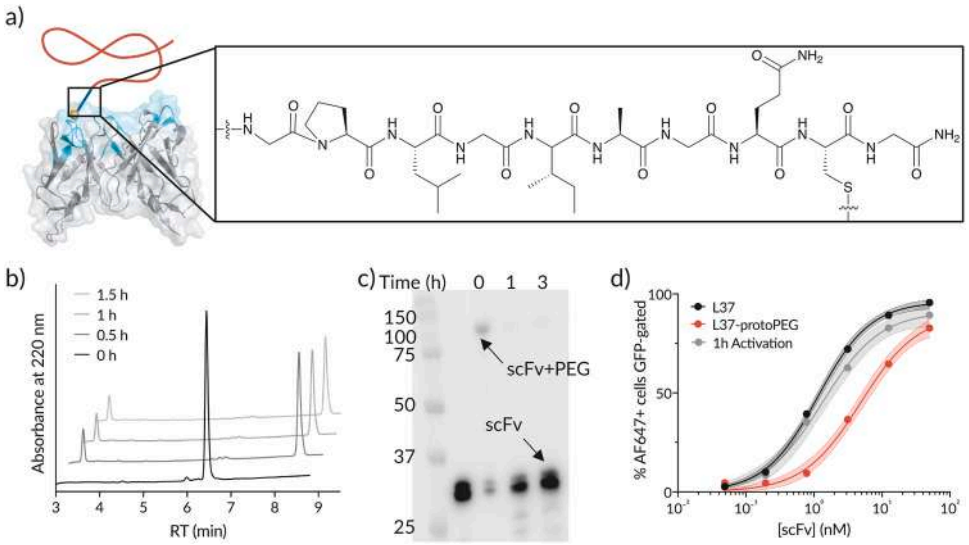


**Fig. 5.** Engineering protease-sensitivity into the masked scFv. a) Sequence of the protease-cleavable linker. b) Cleavage of the synthetised protease-sensitive linker after incubation with MMP2, as assessed by reverse-phase UHPLC. c) Western blot showing conjugation of protease-sensitive 30 kDa PEG to L37 and its cleavage upon incubation with activated MMP2 for 1 and 3 h. Although the amount of sample loaded in lanes 0, 1 and 3 h is the same, the band corresponding to the 30kDa PEG-scFv displays lower intensity because the retention on the blotting membrane of the PEG conjugate is lower than that of the scFv alone. d) Binding of the scFv conjugated to the protease-cleavable PEG with and without incubation with activated MMP2, as assessed by flow cytometry. Filled area indicates the 95% confidence interval for the fitted values. This set of data is representative of 2 independent experiments.

UHPLC. In our hands, the sequence was cleaved more efficiently by MMP-2, so this enzyme was preferentially used for activation in the subsequent experiments (Fig. 5b and Suppl. Fig. S9a-b). After conjugating the protease-sensitive linker to the 30 kDa mPEG-mal in solution, the N-terminus of the peptide was functionalised with a maleimide to enable conjugation with the free Cys on the mutant scFv.

The protease-sensitive PEG linker was conjugated to the L37 scFv mutant and its cleavage by MMP2 was confirmed by WB analysis (Fig. 5c). Binding to HeLa cells overexpressing CD133 was significatively hindered by the mask and, after 1 h incubation in vitro with the catalytic domain of MMP2, the affinity was completely recovered (Fig. 5d).

## Conclusions

In this work, a new versatile approach to generate conditionally-active antibodies is proposed. The strategy relies on site-specific conjugation of reversible polymer masks to the antibody paratope to decrease binding to the antigen. The selection of an optimal conjugation site enables modulation of the masking efficiency with relation to the size of the mask. Moreover, it is shown that, in the presence of specific stimuli, the binding capacity can be rescued. Compared to previously reported strategies, the chemogenetic approach here presented allows readily implementing responsiveness to different stimuli. As a proof of concept, photo- and protease-cleavable masking moieties are utilised. Moreover, since this method only requires an engineered cysteine on the paratope, it has the potential of being applied to different antibody formats and specificities. With this approach, we are one step closer to devising a generalisable masking strategy to develop conditionally-active biotherapeutics.

## Funding

The project that gave rise to these results received the support of a fellowship from "la Caixa" Foundation (ID 100010434) and from the European Union's Horizon 2020 research and innovation programme under the Marie Sklodowska-Curie (MSCA) grant agreement No 847648. R.L., C.D.-P., and B.O.-S. hold FPU (FPU19/03216 MCIN/AEI), MSCA-PF (101063066) and "la Caixa" Junior Leaders (100010434) fellowships, respectively. We also acknowledge support from MCIN/AEI/ 10.13039/501100011033 (PID2020-117486RA-I00), AECC (IDEAS211057OLLE) and AGAUR (SGR-2021-00537).

## Declaration of Competing Interest

No conflict of interest to declare.

## Data availability

Data will be made available on request.

## Acknowledgements

B.O.-S. devised the research project. Experiments were carried out by R.L., M.C.L. and M.E.R. C.D.-P. contributed to the synthesis of the cleavable linkers. The authors acknowledge Dr J. Panyam for kindly providing the anti-CD133 scFv, Dr X. Biarnes-Fontal and A. Querol for generating the model of the structure of the scFv, and Dr M. Artigues for expert advice on the LC-MS analysis. R.L and B.O.-S. wrote the manuscript with input from all authors. All figures were created or modified with Biorender.com.

## Appendix A. Supporting information

Supplementary data associated with this article can be found in the online version at doi:10.1016/j.nbt.2023.10.004.

## References

[1] Lyu X, Zhao Q, Hui J, Wang T, Lin M, Wang K, et al. The global landscape of approved antibody therapies. Antib Ther 2022;5:233. https://doi.org/10.1093/ABT/TBAC021.

[2] Carter PJ, Lazar GA. Next generation antibody drugs: pursuit of the "high-hanging fruit". Nat Rev Drug Discov 2017;17:197–223. https://doi.org/10.1038/nrd.2017.227.

[3] Lucchi R, Bentanachs J, Oller-Salvia B. The masking game: design of activatable antibodies and mimetics for selective therapeutics and cell control. ACS Cent Sci 2021;7:724–38. https://doi.org/10.1021/ACSCENTSCI.0C01448/ASSET/IMAGES/LARGE/OC0C01448_0007.JPEG.

[4] Heo YA. Efgartigimod: first approval. Drugs 2022;82:341–8. https://doi.org/10.1007/S40265-022-01678-3/METRICS.
[5] Heo YA. Satralizumab: first approval. Drugs 2020;80:1477–82. https://doi.org/10.1007/S40265-020-01380-2/METRICS.
[6] McKeage K. Ravulizumab: first global approval. Drugs 2019;79:347–52. https://doi.org/10.1007/S40265-019-01068-2/TABLES/1.
[7] Cattaruzza F, Nazeer A, To M, Hammond M, Koski C, Liu LY, et al. Precision-activated T-cell engagers targeting HER2 or EGFR and CD3 mitigate on-target, off-tumor toxicity for immunotherapy in solid tumors. Nat Cancer 2023;4:485–501. https://doi.org/10.1038/s43018-023-00536-9.
[8] Maejima A, Suzuki S, Makabe K, Kumagai I, Asano R. Incorporation of a repeated polypeptide sequence in therapeutic antibodies as a universal masking procedure: a case study of T cell-engaging bispecific antibodies. New Biotechnol 2023;77:80–9. https://doi.org/10.1016/j.nbt.2023.07.004.
[9] Swaminathan SK, Niu L, Waldron N, Kalscheuer S, Zellmer DM, Olin MR, et al. Identification and characterization of a novel scFv recognizing human and mouse CD133. Drug Deliv Transl Res 2013;3:143. https://doi.org/10.1007/S13346-012-0099-6.
[10] Sun H, Wu GM, Chen YY, Tian Y, Yue YH, Zhang GL. Expression, production, and renaturation of a functional single-chain variable antibody fragment (scFv) against human ICAM-1. Braz J Med Biol Res 2014;47:540–7. https://doi.org/10.1590/1414-431×20143276.
[11] Glumac PM, LeBeau AM. The role of CD133 in cancer: a concise review. Clin Transl Med 2018;7:e18. https://doi.org/10.1186/S40169-018-0198-1.
[12] Yang T, Mochida Y, Liu X, Zhou H, Xie J, Anraku Y, et al. Conjugation of glucosylated polymer chains to checkpoint blockade antibodies augments their efficacy and specificity for glioblastoma. Nat Biomed Eng 2021;5:1274–87. https://doi.org/10.1038/s41551-021-00803-z.
[13] Song SH, Ghosh T, You DG, Joo H, Lee J, Lee J, et al. Functionally masked antibody to uncouple immune-related toxicities in checkpoint blockade cancer therapy. ACS Nano 2022;17:10065–77. https://doi.org/10.1021/ACSNANO.2C12532/ASSET/IMAGES/LARGE/NN2C12532_0004.JPEG.
[14] Zhao Y, Xie YQ, Van Herck S, Nassiri S, Gao M, Guo Y, et al. Switchable immune modulator for tumor-specific activation of anticancer immunity. Sci Adv 2021:7. https://doi.org/10.1126/SCIADV.ABG7291.
[15] Lowman HB, Liu S. Activatable antibodies having non-binding steric moieties for therapy; 9(856), 314 B2; 2018.
[16] Onuoha SC, Ferrari M, Sblattero D, Pitzalis C. Rational design of antirheumatic prodrugs specific for sites of inflammation. Arthritis Rheumatol 2015;67:2661–72. https://doi.org/10.1002/ART.39232.
[17] Oller-Salvia B, Kym G, Chin JW. Rapid and efficient generation of stable antibody-drug conjugates via an encoded cyclopropene and an inverse-electron-demand diels-alder reaction. Angew Chem Int Ed Engl 2018;57:2831–4. https://doi.org/10.1002/ANIE.201712370.
[18] Jumper J, Evans R, Pritzel A, Green T, Figurnov M, Ronneberger O, et al. Highly accurate protein structure prediction with AlphaFold. Nature 2021;596:583–9. https://doi.org/10.1038/S41586-021-03819-2.
[19] Ehrenmann F, Lefranc MP. IMGT/DomainGapAlign: IMGT standardized analysis of amino acid sequences of variable, constant, and groove domains (IG, TR, MH, IgSF, MhSF). Cold Spring Harb Protoc 2011;2011:737–49. https://doi.org/10.1101/PDB.PROT5636.
[20] Ehrenmann F, Kaas Q, Lefranc MP. IMGT/3Dstructure-DB and IMGT/DomainGapAlign: a database and a tool for immunoglobulins or antibodies, T cell receptors, MHC, IgSF and MhcSF. Nucleic Acids Res 2010:38. https://doi.org/10.1093/NAR/GKP946.
[21] Banskota S, Yousefpour P, Kirmani N, Li X, Chilkoti A. Long circulating genetically encoded intrinsically disordered zwitterionic polypeptides for drug delivery. Biomaterials 2019;192:475–85. https://doi.org/10.1016/J.BIOMATERIALS.2018.11.012.
[22] Olszowy M, Nowak-Perlak M, Woźniak M. Current strategies in photodynamic therapy (PDT) and photodynamic diagnostics (PDD) and the future potential of nanotechnology in cancer treatment. Pharmaceutics 2023;15:1712. https://doi.org/10.3390/PHARMACEUTICS15061712.
[23] Fooladi S, Nematollahi MH, Iravani S. Nanophotocatalysts in biomedicine: cancer therapeutic, tissue engineering, biosensing, and drug delivery applications. Environ Res 2023:231. https://doi.org/10.1016/J.ENVRES.2023.116287.
[24] Ibsen S, Zahavy E, Wrasidlo W, Hayashi T, Norton J, Su Y, et al. Localized in vivo activation of a photoactivatable doxorubicin prodrug in deep tumor tissue. Photochem Photobiol 2013;89:698–708. https://doi.org/10.1111/PHP.12045.
[25] Elisseeff J, Anseth K, Sims D, Mcintosh W, Randolph M, Langer R. Transdermal photopolymerization for minimally invasive implantation. Proc Natl Acad Sci USA 1999;96:3104–7. https://doi.org/10.1073/PNAS.96.6.3104/ASSET/14A2C27C–16B8-47FE-8C3D-D3B86E1E04AF/ASSETS/GRAPHIC/PQ0694762003.JPEG.
[26] Engelen W, Zhu K, Subedi N, Idili A, Ricci F, Tel J, et al. Programmable bivalent peptide-DNA locks for pH-based control of antibody activity. ACS Cent Sci 2020;6:22–31. https://doi.org/10.1021/acscentsci.9b00964.
[27] Wouters SFA, Wijker E, Merkx M. Optical control of antibody activity by using photocleavable bivalent peptide–DNA locks. ChemBioChem 2019;20:2463–6. https://doi.org/10.1002/cbic.201900241.
[28] Jiang H, Li H. Prognostic values of tumoral MMP2 and MMP9 overexpression in breast cancer: a systematic review and meta-analysis. BMC Cancer 2021:21. https://doi.org/10.1186/S12885-021-07860-2.
[29] Mook ORF, Frederiks WM, Van Noorden CJF. The role of gelatinases in colorectal cancer progression and metastasis. Biochim Biophys Acta 2004;1705:69–89. https://doi.org/10.1016/J.BBCAN.2004.09.006.
[30] Forsyth PA, Wong H, Laing TD, Rewcastle NB, Morris DG, Muzik H, et al. Gelatinase-A (MMP-2), gelatinase-B (MMP-9) and membrane type matrix metalloproteinase-1 (MT1-MMP) are involved in different aspects of the pathophysiology of malignant gliomas. Br J Cancer 1999;79:1828–35. https://doi.org/10.1038/SJ.BJC.6690291.
[31] Lim M, Jablons DM. Matrix metalloproteinase expression in lung cancer. Methods Mol Med 2003;74:349–56. https://doi.org/10.1385/1-59259-323-2:349/TABLES/1.
[32] Kline T, Torgov MY, Mendelsohn BA, Cerveny CG, Senter PD. Novel antitumor prodrugs designed for activation by matrix metalloproteinases-2 and -9. Mol Pharm 2004;1:9–22. https://doi.org/10.1021/MP0340183.
[33] Albright CF, Graciani N, Han W, Yue E, Stein R, Lai Z, et al. Matrix metalloproteinase-activated doxorubicin prodrugs inhibit HT1080 xenograft growth better than doxorubicin with less toxicity. Mol Cancer Ther 2005;4:751–60. https://doi.org/10.1158/1535-7163.MCT-05-0006.
[34] Desnoyers LR, Vasiljeva O, Richardson JH, Yang A, Menendez EEM, Liang TW, et al. Tumor-specific activation of an EGFR-targeting probody enhances therapeutic index. Sci Transl Med 2013;5:207ra144. https://doi.org/10.1126/scitranslmed.3006682.
[35] Trang VH, Zhang X, Yumul RC, Zeng W, Stone IJ, Wo SW, et al. A coiled-coil masking domain for selective activation of therapeutic antibodies. Nat Biotechnol 2019;37:761–5. https://doi.org/10.1038/s41587-019-0135-x.
[36] Kratz F, Drevs J, Bing G, Stockmar C, Scheuermann K, Lazar P, et al. Development and in vitro efficacy of novel MMP2 and MMP9 specific doxorubicin albumin conjugates. Bioorg Med Chem Lett 2001;11:2001–6. https://doi.org/10.1016/S0960-894X(01)00354-7.